Electromagnetic Analysis for Multi-Constellation GNSS Satellite Visibility Determination in Urban Areas

Wei-Jiang Zhao, **Binfang Wang**, **and En-Xiao Liu**

Institute of High Performance Computing, A*STAR, Singapore

Abstract— The satellite visibility of global navigation satellite systems in urban areas is investigated with electromagnetic ray-based methods and 3D city models. The satellite position is computed with satellite orbital parameters and the SGP4 standard mathematical model of satellite orbits. The obstruction, reflection and diffraction of satellite signals due to the presence of buildings are taken into account in the prediction of satellite visibility, with the satellite signal propagation paths being determined by using the ray tracing and 3D city models. In some cases where it is hard for a receiver to detect a satellite due to too low signal level, there do exist predicted signal propagation paths from the satellite to the receiver via reflection or diffraction. The received signal level is also estimated with the electromagnetic ray-based methods to enable the predicted satellite visibility to be correlated with that observed.

1. INTRODUCTION

Global navigation satellite systems, GNSS in short, are satellite-based radio navigation systems that provide geolocation and time information to a GNSS receiver anywhere near or on the earth. Satellite visibility represents the ability of a receiver to sense a signal from a satellite. A GNSS receiver typically requires a clear radio channel to at least four GNSS satellites. In urban areas with high-rise, high density residential and commercial development, so-called urban canyons, tall buildings often block the direct line-of-sight (LOS) signals from many GNSS satellites, leading to either poor GNSS positioning accuracy or lack of a positioning solution. Many satellite visibility tool available online such as *CalSky* have been developed for providing the coverage information for satellite constellations without considering satellite signal obstruction. Actual satellite visibility in urban areas generally becomes worse due to the presence of tall buildings. Recently, three-dimensional (3D) building models have been utilized to predict satellite visibility in urban areas, with the purpose to correct the multipath errors by identifying and removing reflection paths or to find a possible positioning solution in urban canyons via utilizing reflection paths [1, 2]. The diffraction by building wedges and the received satellite signal strength are seldom considered in the prediction. Also, most satellite visibility predictions utilize the GNSS ephemeris and almanacs orbital parameter data to compute the satellite position. However, the data are difficult to obtain for BeiDou and QZSS satellite systems.

In this paper, the prediction of satellite visibility in urban areas is investigated for five GNSS constellations including GPS, GLONASS, Galileo, BeiDou and QZSS. The two-line element set (TLEs) orbital parameter data that are available online for all considered GNSS constellations are employed to compute the satellite position with the SGP4 standard mathematical model of satellite orbits [3, 4]. The consideration of multi-constellation navigation satellite systems increases the number of satellites in the field of view, alleviating the problems caused by building obstruction and improving spatial distribution of visible satellites. Electromagnetic ray-based methods combined with 3D city models are employed to model the satellite signal propagation in complicated urban environment. The signal obstruction, reflection and diffraction by buildings are considered [5, 6, 7, 8]. The 3D city models used here are those in the stereolithography (STL) format represented by unstructured surfaces [9]. Real-world observation by using a GNSS receiving device is conducted to verify the predicted satellite visibility results.

2. SATELLITE POSITION AND 3D CITY MODELS

2.1. Satellite Position

The prediction of the GNSS satellite visibility needs the knowledge of satellite position which can be computed from the orbital properties of the satellites in TLEs format with the SGP4 standard mathematical model of satellite orbits [4]. The TLEs data which are updated regularly can be

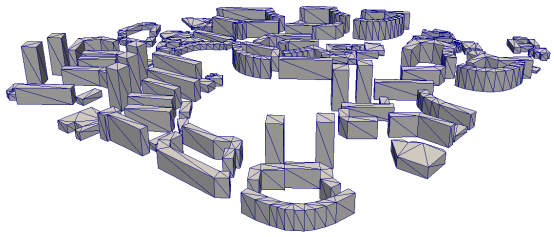

Figure 1: 3D city model for an urban district in STL format.

downloaded and their widespread availability for all GNSS is the primary reason why the TLEs is chosen in this work. Table 1 gives the description of TLEs orbital parameters used for computing the satellite position.

Table 1: TLEs format and description of items.

Field	Column	Item
1.1	1	Line Number of Element Data
1.7	19-20	Epoch Year (Last two digits of year)
1.8	21-32	Epoch (Day of the year and fractional portion of the day)
2.1	1	Line Number of Element Data
2.3	9-16	Inclination in Degrees
2.4	18-25	Right Ascension of the Ascending Node in Degrees
2.6	35-42	Argument of Perigee in Degrees
2.7	44-51	Mean Anomaly in Degrees
2.8	53-63	Mean Motion [Revs per day]

2.2. 3D City Models

3D city models in the STL format is employed, which can be obtained from CityGML or 3DS models by conversion. An STL file describes only the surface geometry of a 3D object without any CAD model attributes, and it contains the information of unstructured triangulated surface by the unit normal and vertices (ordered by the right-hand rule) of the triangles. An STL model of an urban district is displayed in Fig. 1.

3. ELECTROMAGNETIC RAY-BASED METHODS

Electromagnetic ray-based methods such as the uniform theory of diffraction (UTD) are based on rays of direct incidence, reflection and diffraction [7, 8]. The propagation paths relating to these rays are first determined. A ray is included to compute the received signal strength if it exists and is not obstructed. A GNSS receiving device can receive both (direct) LOS and non-LOS (reflection or diffraction) rays.

3.1. Propagation Path Determination

A direct ray from a satellite to a receiver exists if it is not obstructed by any building. The shadowing algorithm presented in [5] is employed to check if a direct ray is obstructed.

To determine a reflected path, it is needed to find a reflected point on a reflected surface. The image-based ray tracing technique presented in [6] is well suited for determining reflected points and reflected paths. A predicted reflection path from a satellite to a receiver passing through a reflected point is an effective propagation path only when the reflected point is visible to both the satellite and the receiver.

Similarly, it is needed to find a diffracted point over a diffracted edge in the determination of a diffracted ray. this can be done by the following proposed algorithm. Let S and R denote the positions of satellite and receiver, respectively, V_1 and V_2 the two vertices of an edge, Q the diffracted point on the edge, and O the origin of the coordinate system, as shown in Fig. 2. Because

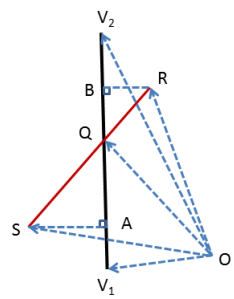

Figure 2: The geometry for determining a diffracted point.

Q is on the edge V_1V_2 and it is on the line SR as well, we have

$$\overline{OQ} = \overline{OV_1} + t(\overline{OV_2} - \overline{OV_1}), \tag{1}$$

and

$$\overline{OQ} = \overline{OS} + p(\overline{OR} - \overline{OS}), \tag{2}$$

as where t and p are real numbers between 0 and 1. Let A and B be the points on the edge that make the lines SA and RB be normal to the edge V_1V_2. As the angle formed by the incident ray and the edge equals that formed by the diffracted rays and the edge, SQA and RQB are similar triangles and this results in

$$\frac{p}{1-p} = \frac{|\overline{SA}|}{|\overline{RB}|}, \tag{3}$$

and thus p can be expressed as

$$p = \frac{|\overline{SA}|}{|\overline{SA}| + |\overline{RB}|}. \tag{4}$$

Substituting (4) and (2) into (1), we derive the expression of t

$$t = \frac{\overline{V_1V_2}}{|\overline{V_1V_2}|^2} \cdot (\frac{|\overline{RB}|\overline{OS} + |\overline{SA}|\overline{OR}}{|\overline{SA}| + |\overline{RB}|} - \overline{OV_1}). \tag{5}$$

The right-hand side of (5) is known. Once t is obtained, we can compute the diffracted point with (1). If the diffracted point is visible to both the satellite and the receiver, the associated diffracted path is an effective propagation path from the satellite to the receiver passing through the diffracted point. Fig. 3 shows the comparison of the predicted and observed satellite visibility, where the diffraction is not taken into account in the initial prediction. It can be seen that all the GPS and GLONASS satellites in the figure are both predicted and observed except the GPS satellite 'G29', and the predicted and observed satellite positions also agree well with each other. After including the diffraction effect in the prediction, 'G29' becomes predictable.

3.2. Signal Strength Calculation

The field reflected by dielectric surfaces can be easily computed once the reflection path is determined [6]. The building surfaces with two different dielectric materials, i.e., concrete and glass, are considered. The dielectric properties used for the reflection computation are those recommended by the International Telecommunications Union (ITU). Both materials have a dielectric constant of 7, and the loss tangent for the concrete and glass are 0.12 and 0.014, respectively. Fig. 4 shows the computed reflection coefficients versus the angle of incidence, where the TE and TM polarizations stand for the incident electric field perpendicular and parallel to the incident plane formed by the incident ray and surface normal, respectively. It can be seen that the concrete surface generally has 2 dB higher reflection attenuation than the glass surface.

The computation of the field diffracted by dielectric wedges is relatively complicated. After investigating various UTD diffraction coefficients for dielectric wedges, we employ heuristic UTD coefficients introduced in [7] that are given by

$$D_{s,h} = H_{s,h}D_1 + D_2 + R_{s,h}(\alpha_n)D_3 + R_{s,h}(\alpha_0)D_4, \tag{6}$$

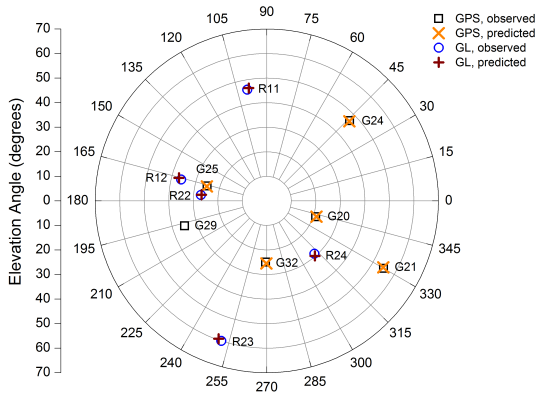

Figure 3: Comparison of predicted and observed satellite visibility.

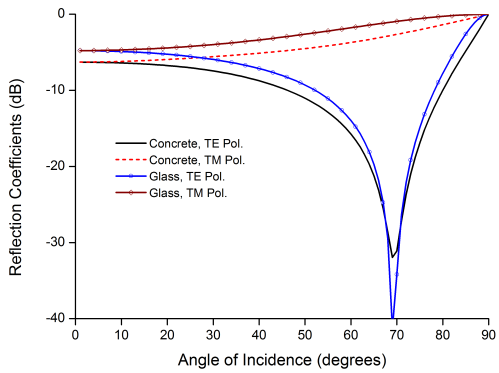

Figure 4: Reflection coefficients for the concrete and glass building surfaces.

where D_1, D_2, D_3, and D_4 are the four terms of usual UTD diffraction coefficients defined in [8], and $R_{s,h}(\alpha_n)$ and $R_{s,h}(\alpha_0)$ represent the Fresnel reflection coefficients associated with the n and 0 dielectric wedge faces, respectively. The subscripts s and h represent soft and hard polarization, respectively, with the former referring to the incident electric field normal to the incident plane, and the latter referring the incident electric field parallel to the incident plane. $H_{s,h}$ is given by

$$H_{s,h} = R_{s,h}(\alpha_n)R_{s,h}(\alpha_0). \tag{7}$$

Fig. 5 shows the computed UTD diffraction coefficients for a concrete wedge with the exterior wedge angle being 270°, where the angle of incidence ϕ_i is 45°. The coefficients for the same wedge with perfect electric conductor (PEC) wedge faces are also computed and plotted in the same figure for reference. It can be seen that, in the shadow region where $\phi_i > 225°$, the hard polarization component is greater than the soft polarization component, and the attenuation due to the diffraction by the concrete wedge is obviously higher than that due to the direction by the PEC wedge for the primary polarization.

4. CONCLUSION

The electromagnetic ray-based methods are applied to the prediction of GNSS satellite visibility. In the case of direct signal from a satellite is blocked by buildings, a GNSS receiver may still detect the satellite via reflected or diffracted signals. After taking into account the reflection and diffraction, better agreement between the predicted and the observed satellite visibility can be achieved. In the shadow region, the attenuation due to the diffraction by a concrete wedge is obviously higher than that due to the diffraction by a PEC wedge for the soft polarization.

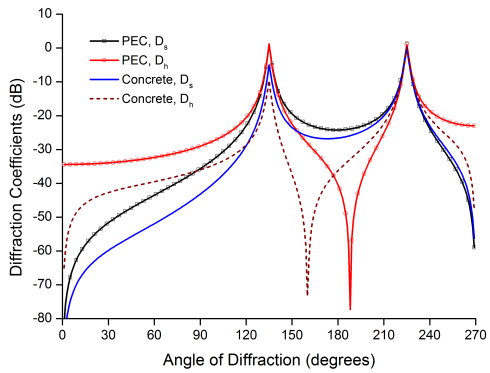

Figure 5: Diffraction coefficients for concrete and PEC wedges.

ACKNOWLEDGMENT

This work was supported (in part) by National Research Foundation under Virtual Singapore Program Award No. NRF2017VSG-AT3DCM001-038. The authors would like to thank Mr. Tan Chee Boon, Wayne from the GoveTech, Singapore and Dr. Shen Chongjiang from the National University of Singapore for providing the measured satellite visibility results.

REFERENCES

1. Wang, L., Groves, P. D. & Ziebart, K., "GNSS shadow matching: Improving urban positioning accuracy using a 3D city model with optimized visibility prediction scoring," *25th Int. tech. Meeting of the Satellite Division of the ION*, Nashville TN, USA, September 17-21, 2012, 423-437.
2. Germroth, M. & Carstensen, L., "GIS and satellite visibility: Viewsheds from space," *Proc. 2005 ESRI International User Conference*, July 25-29, 2005.
3. Carrico, T., Carrico, J., Policastri, L., & Loucks, M., "Investigating orbital debris events using numerical methods with full force model orbit propagation," *American Institute of Aeronautics and Astronautics* , Vol. 128, No. 8, 2008.
4. Vallado, D. A., Crawford, P., Hujsak, R., & Kelso, T. S., "Revisiting Spacetrack Report #3," *Astrodynamics Specialist Conference and Exhibit*, Keystone, Colorado, August 21-24, 2006.
5. Wang, B. F. & Zhao, W. J., "Analysis of high-frequency electromagnetic scattering by complex targets using dual flat facet representation," *IEEE Transactions on Antennas and Propagation*, Vol. 63, No. 11, 4976–4982, 2015.
6. Zhao, W. J., Liu, E. X., Wang, B. F., Gao, S. P., & Png, C. E., "An approach combining the integral equation method with a generalized image technique for modeling incabin radio wave propagation," *International Journal of Numerical Modelling Electronic Networks Devices and Fields*, in press, 2019.
7. Schettino, D. N., Moreira, F. J.S., & Rego, C. G., "Heuristic UTD coefficients for electromagnetic scattering by lossy conducting wedges," *Microwave and Optical technology Letters*, Vol. 52, No. 12, 2657-2662, December 2010.
8. Kouyoumjian, R. & Pathak, P., "A uniform geometrical theory of diffraction for an edge in a perfectly conducting surface," *Proc. IEEE*, Vol. 62, 1448-1461, 1974.
9. Zhao, W. J., Liu, E. X., Poh, H. J., Wang, B. F., Gao, S. P., Png, C. E., Li, W. H., & Chong, S. H., "3D traffic noise mapping using unstructured surface mesh representation of buildings and roads," *Applied Acoustics*, Vol. 127, No. 12, 297-304, 2017.